J|A|C|S
ARTICLES
Published on Web 06/06/2006

Two-State Reactivity, Electromerism, Tautomerism, and "Surprise" Isomers in the Formation of Compound II of the Enzyme Horseradish Peroxidase from the Principal Species, Compound I

Etienne Derat and Sason Shaik*

Contribution from the Department of Organic Chemistry and the Lise Meitner-Minerva Center for Computational Quantum Chemistry, Hebrew University of Jerusalem, Givat Ram Campus, 91904 Jerusalem, Israel

Received January 5, 2006; E-mail: sason@yfaat.ch.huji.ac.il

Abstract: QM and QM/MM calculations on Compound II, the enigmatic species in the catalytic cycle of the horseradish peroxidase enzyme, reveal six low-lying isomers. The principal isomer is the triplet oxo-ferryl form ($PorFe^{IV}$═O) that yields the hydroxo-ferryl isomer ($PorFe^{IV}$—OH^{+}). These are the only forms observed in experimental studies. Theory shows, however, that these are *the least stable isomers of Compound II*. The two most stable forms are the singlet and triplet states of the $Por^{+\bullet}Fe^{III}$—OH electromer. In addition, theory reveals species never considered in heme enzymes: the singlet and triplet states of the $Por^{+\bullet}Fe^{III}$—OH_2 electromer. The computational results reproduce the experimental features of the known isomers and enable us to draw relationships and make predictions regarding the missing ones. For example, while the "surprise" species, singlet and triplet $Por^{+\bullet}Fe^{III}$—OH_2, have never been considered in heme chemistry, the calculated Fe−O bond lengths indicate that these isomers may have, in fact, been observed in one of the two opposing EXAFS studies reported previously. Furthermore, these ferric-aqua complexes could be responsible for the reported ^{18}O exchange with bulk water. It is clear, therefore, that the role of Compound II in the HRP cycle is considerably more multi-faceted than has been revealed so far. Our suggested multi-state reactivity scheme provides a paradigm for Compound II species. The calculated Mössbauer parameters may be helpful toward eventual characterization of these missing isomers of Compound II.

Introduction

Peroxidases are metalloenzymes that utilize two active species in their catalytic cycle (Scheme 1), one called Compound I (Cpd I, **1** in Scheme 1) and the other Compound II (Cpd II, **2a** and **2b** in Scheme 1). These two species involve iron ions in a high-valence state, storing, respectively, two and one oxidation equivalents that are utilized to oxidize substrates and perform, thereby, biologically vital processes.[1,2] The structure of Cpd I is well established,[1−4] and with the exception of cytochrome *c* peroxidases,[5] Cpd I species involve an oxo-ferryl ($Fe^{IV}O$) moiety embedded in a porphyrin radical-cationic ($Por^{+\bullet}$) macrocycle. As shown in Scheme 2, Cpd I involves three unpaired electrons, two on the π^* orbitals of the oxo-ferryl unit and one in an a_{2u} orbital on the $Por^{+\bullet}$ macrocycle, giving rise to two closely lying spin states, quartet ($S = {}^3/_2$) and doublet ($S = {}^1/_2$).

Scheme 1. Schematic Catalytic Cycle of Peroxidases

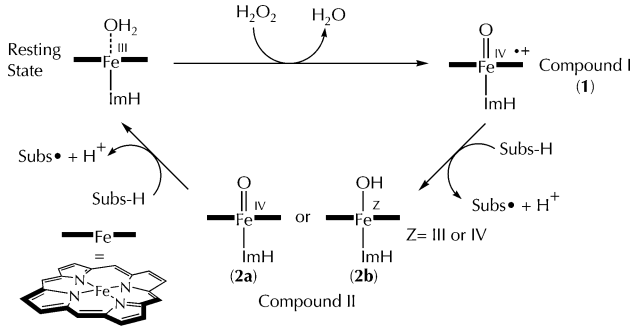

By comparison, the structure of Cpd II is more complex due to the potential availability of multiple forms. In principle, Cpd II is generated from Cpd I by one-electron reduction, but since a proton can be released during the substrate oxidation (Scheme 1), the reduction of Cpd I may be attended by protonation, either simultaneously or in a subsequent step. This yields oxo-ferryl (**2a**) and/or the hydroxo-ferryl (**2b**) species; the latter has, in fact, two electromers[6] and two possible spin states.[6c,d] Thus, as shown in Scheme 2, the ground state of the oxo-ferryl species, **2a**, has two electrons occupying the π^* orbitals of the $Fe^{IV}O$

(1) (a) Meunier, B. *Chem. Rev.* **1992**, *92*, 1411−1456. (b) Poulos, T. L. Peroxidases and Cytochrome P450. In *The Porphyrin Handbook*; Kadish, K. M., Smith, K. M., Guilard, R., Eds.; Academic Press: San Diego, 2000; Vol. 4, Chapter 32, pp 189−218. (c) *Handbook of Metalloproteins*; Messerschmidt, A., Huber, R., Poulos, T. L., Wieghardt, K., Eds.; John-Wiley and Sons: New York, 2001; Vol. 1, pp 193−328 (for HRP in particular, see the section by M. Gajhede, pp 195−209). (d) Dawson, J. H.; Sono, M. *Chem. Rev.* **1987**, *87*, 1255−1276. (e) Dawson, J. H. *Science* **1988**, *240*, 433−439. (f) Colas, C.; Ortiz de Montellano, P. R. *Chem. Rev.* **2003**, *103*, 2305−2332.
(2) Dunford, H. B. *Heme Peroxidases*; Wiley-VCH: New York, 1999.
(3) Dawson, J. H.; Sono, M. *Chem. Rev.* **1987**, *87*, 1255−1276.
(4) Harris, D. L. *Curr. Opin. Chem. Biol.* **2001**, *5*, 724−735.
(5) Bonagura, C. A.; Bhaskar, B.; Shimizu, H.; Li, H.; Sundaramoorthy, M.; McRee, D. E.; Goodin, D. B.; Poulos, T. L. *Biochemistry* **2003**, *42*, 5600−5608.

Scheme 2. Electronic Structures of the **2a** and **2b** Forms of Cpd II in Two Spin States

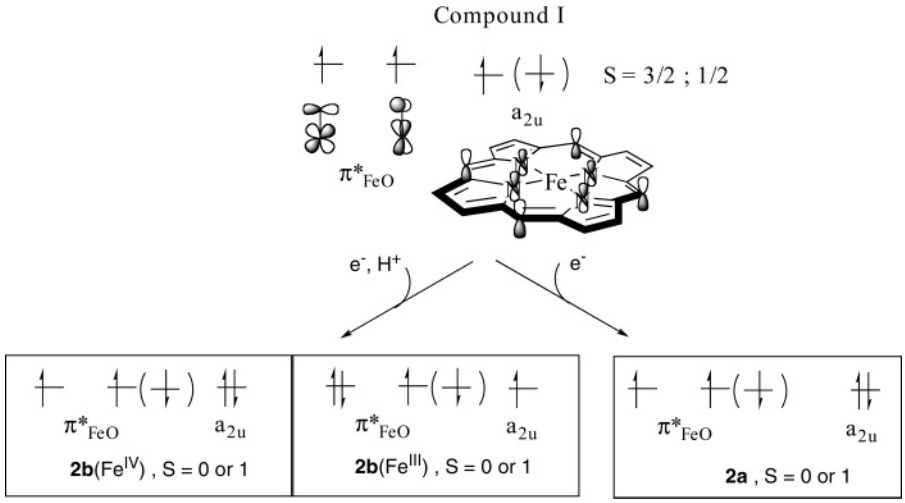

moiety with a triplet spin quantum number ($S = 1$); the corresponding singlet state ($S = 0$) is an excited state. The hydroxo-ferryl species possesses two electromers: one, $PorFe^{IV}$—OH (**2b**(Fe^{IV})), has a triplet ground state, and the other, $Por^{+\bullet}$-Fe^{III}—OH (**2b**(Fe^{III})), has two closely lying spin states, triplet and singlet.[6c,d] As such, the reduction, with or without protonation, of Cpd I to form Cpd II may involve two spin states, two different species, and at least two electromers. There is then a two-pronged problem associated with Cpd II: the first question concerns the relative stability of all these forms and the identity of the ground state, and the second question concerns the formation of these species from Cpd I and their potential interconversion. Since Cpd II is essential for the reactivity of the enzyme and for the completion of its catalytic cycle, it is necessary to establish the relationships between all these forms of the active species. This paper addresses these questions for the enzyme horseradish peroxidases (HRP), where a good measure of uncertainty exists regarding the identity of the Cpd II species and its multiple forms. As shall be seen, even this long-standing problem harbors some surprises, including new species.

A Brief Review of Existing Data on Cpd II. Let us review first some of the problems associated with Cpd II of HRP. Isotope labeling[7] shows that Cpd I of HRP contains a single oxygen atom, and since Cpd II is obtained from Cpd I by reduction, this has been considered to be also the constitution of Cpd II that could either be an oxo-ferryl or a hydroxo-ferryl species. Structure determination by EXAFS led, indeed, to differing conclusions: some studies[8] conclude that Cpd II possesses a short Fe−O bond, ca. 1.60−1.70 Å, corresponding to an oxo-ferryl species, **2a**, while other studies[9] find that the species has a very long Fe−O bond of 1.92−1.93 Å, hence corresponding presumably to a hydroxo-ferryl type, with a formal single Fe−O bond. An X-ray structural determination shows that Cpd II is generated from Cpd I rapidly and has an Fe−O bond length of 1.80 Å[10] that fits a hydroxo-ferryl species, **2b**, but this bond length is significantly shorter than the EXAFS datum (1.92−1.93 Å).[9] Interestingly, an X-ray investigation of myoglobin Cpd II reveals a long Fe−O bond, ca. 1.92 Å, similar to the EXAFS datum for HRP Cpd II.[11a] The electromeric identity of this latter species has been recently studied by combining QM/MM calculations with X-ray data refinement;[11b] the authors gave an assignment of $PorFe^{IV}$—OH, although an Fe^{III}—OH assignment was not ruled out.

In contrast to structural techniques, NMR spectroscopy[12] favors the $PorFe^{IV}$═O assignment. Mössbauer spectroscopy[13] prefers the same assignment, revealing a ferryl (Fe^{IV}) species that has a t_{2g}^4 electronic configuration and an axial symmetry, hence corresponding to $PorFe^{IV}$═O. Similarly, Raman spectroscopy generally prefers the oxo-ferryl tautomer, **2a**.[14] Nevertheless, the Raman data show sensitivity of the Fe−O stretching frequency to the pH of the medium, which is taken as evidence for the existence of a hydrogen-bonded and a free $PorFe^{IV}$═O species; the existence of a $PorFe^{IV}$—OH species was either ruled out or not considered. The existence of two forms of Cpd II in different pH regions was deduced also from the pH dependence of the activity of Cpd II and from its reduction

(6) (a) See: Groves, J. T.; Gross, Z.; Stern, M. K. *Inorg. Chem.* **1994**, *33*, 5065−5072 and references therein. (b) Scheidt W. R.; Reed C. A. *Chem. Rev.* **1981**, *81*, 543−555. (c) Filatov, M.; Harris, N.; Shaik, S. *Angew Chem., Int. Ed.* **1999**, *38*, 3510−3512. (d) Shaik, S.; Cohen, S.; de Visser S. P.; Sharma, P. K.; Kumar D.; Kozuch S.; Ogliaro F.; Danovich D. *Eur. J. Inorg. Chem.* **2004**, 207−226.

(7) (a) Schonbaum, G. R.; Lo, S. *J. Biol. Chem.* **1972**, *247*, 3353−3360. (b) Hager, L. P.; Doubek, D. L.; Silverstein, R. M.; Hargis, J. H.; Martin, J. C. *J. Am. Chem. Soc.* **1972**, *94*, 4364−4366. (c) Felton, R. H.; Romans, A. Y.; Yu, N.-T.; Schonbaum G. R. *Biochim. Biophys. Acta* **1976**, *434*, 82−89. (d) Roberts, J. E.; Hoffman, B. M.; Rutter, R.; Hager, L. P. *J. Am. Chem. Soc.* **1981**, *103*, 7654−7656.

(8) (a) Penner-Hahn, J. E.; Eble, K. S.; McMurry, T. J.; Renner, M.; Balch, A. L.; Groves, J. T.; Dawson, J. H.; Hodgson, K. O. *J. Am. Chem. Soc.* **1986**, *108*, 7819−7825. (b) Green, M. T.; Dawson, J. H.; Gray H. B. *Science* **2004**, *304*, 1653−1656. (c) Penner-Hahn, J. E.; McMurry, T. J.; Renner, M.; Latos-Grazynsky, L.; Eble, K. S.; Davis, I. M.; Balch, A. L.; Groves, J. T.; Dawson, J. H.; Hodgson, K. O. *J. Biol. Chem.* **1983**, *258*, 12761−12764.

(9) (a) Chance, B.; Powers, L.; Ching, Y.; Poulos, T.; Schonbaum, G. R.; Yamazaki, I.; Paul, K. G. *Arch. Biochem. Biophys.* **1984**, *235*, 596−611. (b) Chance, M.; Powers, L.; Poulos, T.; Chance, B. *Biochemistry* **1986**, *25*, 1266−1270.

(10) Berglund, G. I.; Carlsson, G. H.; Smith, A. T.; Szöke, H.; Henriksen, A.; Hajdu, J. *Nature* **2002**, *417*, 463−468.

(11) (a) Hersleth, H.-P.; Dalhus, B.; Görbitz, C. H.; Andersson, K. K. *J. Biol. Inorg. Chem.* **2002**, *7*, 299−304. (b) Nilsson, K.; Hersleth, H.-P.; Rod T. H.; Andersson K. K.; Ryde U. *Biophys. J.* **2004**, *87*, 3437−3447.

(12) La Mar, G. N.; De Ropp, J. S.; Latos-Grazynski, L.; Balch, A. L.; Johnson, R. B.; Smith, K. M.; Parish, D. W.; Cheng, R. J. *J. Am. Chem. Soc.* **1983**, *105*, 782−787.

(13) Schulz, C. E.; Rutter, R.; Sage, J. T.; Debrunner, P. G.; Hager, L. P. *Biochemistry* **1984**, *23*, 4743−4754.

(14) (a) Kincaid, J. R.; Zheng, Y.; Al-Mustafa, J.; Czarnecki, K. *J. Biol. Chem.* **1996**, *271*, 28805−28811. (b) Sitter, A. J.; Reczek, C. M.; Terner, J. *J. Biol. Chem.* **1985**, *260*, 7515−7522. (c) Makino, R.; Uno, T.; Nishimura, Y.; Iizuka, T.; Tsuboi, M.; Ishimura, Y. *J. Biol. Chem.* **1986**, *261*, 8376−8382. (d) Reczek, C. M.; Sitter, A. J.; Terner, J. *J. Mol. Stuct.* **1989**, *214*, 27−41.

potential to the resting ferric (Fe^{III}) state.[15] Thus, whereas "the acidic Cpd II form" (pH $\leq$ 7) is easier to reduce to the resting state[15b] and it exchanges ^{18}O with the bulk water,[15c] "the basic Cpd II form" is harder to reduce, and it does not exchange ^{18}O. Furthermore, even the activity of Cpd II toward oxidizable substrates depends on the pH of HRP, but there is no clear-cut trend, as in some cases the activity requires acidic pH, while in others a more basic pH is required.[15a,16] Considering all these data, Andersson and Dawson[16] suggested that this sensitivity of the properties of HRP Cpd II is in line with the observation of two very different Fe−O bond lengths in two EXAFS studies, one belonging to Fe^{IV}═O and the other to Fe^{IV}—OH.[8a,9a] Nevertheless, these authors conclude that more experiments will be needed to resolve this dilemma of HRP Cpd II.

Interestingly, two forms of Cpd II are also suggested from magnetic circular dichroism spectra[17] of the species of myoglobin; the two species have triplet ground states with zero-field splitting parameters that depend on the pH, the one in acidic pH resembling the zero-field splitting in Cpd II of HRP.[18] However, the difference between the acidic and alkaline forms is not conclusive, and the alkaline environment is thought to cause deprotonation of either the imidazole proximal ligand or the distal His residue.[17]

Regarding the spin quantum number, magnetic susceptibility measurements[19] suggested a triplet state ($S = 1$), even though the measured magnetic moment was significantly larger than the theoretical one expected for two electrons; presumably this deviation originated in "incomplete quenching of orbital angular momentum".[19b] Interestingly, *none of the experimental studies refers to the* $Por^{+\bullet}Fe^{III}$*—OH electromer, even though such an electromer was generated in solution in synthetic complexes.*[6a]

To summarize the experimental data, it appears that the oxo- and hydroxo-ferryl tautomers of HRP Cpd II may coexist, but there are a few questions that need to be answered: Which form is the ground state of the complex, oxo-ferryl (**2a**) or hydroxo-ferryl (**2b**), and what is the oxidation state in the latter tautomer, **2b**(Fe^{IV}) or **2b**(Fe^{III})? What would be the spin quantum number in the case that the **2b**(Fe^{III}) electromer were to be found the ground state of Cpd II, and what would then be the nature of the conversion of **2a** to **2b**, and does it involve two-state reactivity? What is the reason that the ferric electromer of **2b** has never been detected or reported for HRP Cpd II, while it exists for synthetic complexes?[6a] Why do the great majority of synthetic Cpd II species have the oxo-ferryl form?[8,9,20] Are there any other Cpd II species that do not appear in Scheme 2 and that have not been recognized before?

Theory has been generally very useful in addressing electronic structures and properties of Cpd II models of HRP by means of quantum mechanics using density functional theory (DFT).[21] It is apparent, however, that the above questions concerning HRP Cpd II can be satisfactorily tackled only by those theoretical means that take into account the essential residues of the protein environment as well as its bulk polarity and hydrogen-bonding effects. This is the main goal of this paper, which employs the hybrid quantum mechanical/molecular mechanical method to study the electronic states and interconversion of the various forms of HRP Cpd II, to reveal possible new isomers, and to characterize their Mössbauer spectroscopic parameters.[13,21e,22]

Methodology

The study described herein involves quantum mechanical (QM) as well as hybrid quantum mechanical/molecular mechanical (QM/MM) calculations. The initial QM calculations were used to ascertain the electronic structure and inherent preference of the electromers and tautomers of Cpd II. Subsequently, the QM/MM method was employed to investigate the role of the protein environment in the distal and proximal sides of the heme. An attempt to trace the protonation process from **2a** to **2b** revealed two new "surprise" species. Finally, the QM/MM structures were employed to calculate Mössbauer parameters, as potential probes that can distinguish the various forms of HRP Cpd II, and to assist in their probing by experimental means. The complete data set is collected in the Supporting Information (SI) document.

A. QM Methodology. All calculations were carried out with the hybrid unrestricted B3LYP functional[23] (hence UB3LYP) on the bare oxo-ferryl porphyrin or hydroxo-ferryl porphyrin species. For geometry optimization and frequency calculations, we used the effective core potential on iron and the double-ζ LACVP basis set,[24] coupled with the 6-31G basis-set[25] for all other atoms, henceforth B1. Subsequent single-point calculations were done with the larger basis set, LACV3P+*,[26] designated as B2. These single-point results are abbreviated as B2//B1.

All geometry optimizations and single-point energy calculations were performed with the JAGUAR 5.5 package.[27] To gauge the accuracy of UB3LYP for the problem at hand, single points were done with two other functionals, UB3P86[28] and UMPW1K,[29] on the different spin states and electromers of the two forms, **2a** and **2b**. A test of the accuracy of UB3LYP was

(15) (a) See pp 82−84 in ref 2. (b) Hayashi, Y.; Yamazaki, I. *J. Biol. Chem.* **1979**, *254*, 9101−9106. (c) Hashimoto, S.; Tatsuno, Y.; Kitagawa, T. *Proc. Natl. Acad. Sci. U.S.A.* **1986**, *83*, 2417−2421.
(16) Andersson, L. A.; Dawson, J. H. *Struct. Bonding* **1990**, *74*, 1−40.
(17) Foote, N.; Gadsby, P. M. A.; Greenwood, C.; Thomson, A. J. *Biochem. J.* **1989**, *261*, 515−522.
(18) Browett, W. R.; Gasyna, Z.; Stillman, M. J. *J. Am. Chem. Soc.* **1988**, *110*, 3633−3640.
(19) (a) Theorell, H.; Ehrenberg, A.; Chance, B. *Arch. Biochem. Biophys.* **1952**, *37*, 237−239. (b) Theorell, H.; Ehrenberg, A. *Arch. Biochem. Biophys.* **1953**, *41*, 442−461.
(20) (a) For a non-heme Cpd II, see: Rohde, J.-U.; In, J.-H.; Lim, M. H.; Brennessel, W. W.; Bukowski, M. R.; Stubna, A.; Münck, E.; Nam, W.; Que, L., Jr. *Science* **2003**, *299*, 1037−1039. (b) For heme Cpd II models, see: Chin, D. H.; La Mar, G. N.; Balch, A. L. *J. Am. Chem. Soc.* **1980**, *102*, 1446−1448. Chin, D. H.; La Mar, G. N.; Balch, A. L. *J. Am. Chem. Soc.* **1980**, *102*, 4344−4350. Schappacher, M.; Weiss, R.; Monteil-Montoys, R.; Trautwein, A.; Tabard, A. *J. Am. Chem. Soc.* **1985**, *107*, 3736−3738.
(21) (a) Filatov, M.; Harris, N.; Shaik, S. *J. Chem. Soc., Perkin Trans.* **1999**, *2*, 399−411. (b) Rydberg, P.; Sigfridsson, E.; Ryde, U. *J. Biol. Inorg. Chem.* **2004**, *9*, 203−223. (c) Kuramochi, H.; Noodleman, L.; Case, D. A. *J. Am. Chem. Soc.* **1997**, *119*, 11442−11451. (d) Antony, J.; Grodzicki, M.; Trautwein, A. X. *J. Phys. Chem. A* **1997**, *101*, 2692−2701. (e) Loew, G.; Herman, Z. S. *J. Am. Chem. Soc.* **1980**, *102*, 6173−6174. (f) For recent QM/MM calculations of Cpd I species of APX and CcP, see: Bathelt, C. M.; Mulholland, A. J.; Harvey, J. N. *J. Chem. Soc., Dalton Trans.* **2005**, 3470−3476. (g) Rovira, C.; Fita, I. *J. Phys. Chem. B* **2003**, *107*, 5300−5305. (h) Ghosh, A.; Almlöf, J.; Que, L., Jr. *J. Phys. Chem.* **1994**, *98*, 5576−5579. (i) For a recent QM/MM study of Cpd II of Myoglobin, see ref 11b.
(22) Schünemann, V.; Winkler, H. *Rep. Prog. Phys.* **2000**, *63*, 263−353.
(23) (a) Becke, A. D. *Phys. Rev. A* **1988**, *36*, 3098−3100. (b) Lee, C.; Yang, W.; Parr, R. G. *Phys. Rev. B* **1988**, *37*, 785−789. (c) Becke, A. D. *J. Chem. Phys.* **1993**, *98*, 5648−5652.
(24) (a) Hay, J. P.; Wadt, W. R. *J. Chem. Phys.* **1985**, *82*, 299−310. (b) Friesner, R. A.; Murphy, R. B.; Beachy, M. D.; Ringlanda, M. N.; Pollard, W. T.; Dunietz, B. D.; Cao, Y. X. *J. Phys. Chem. A* **1999**, *103*, 1913−1928.
(25) Hehre, W. J.; Ditchfield, R.; Pople, J. A. *J. Chem. Phys.* **1972**, *56*, 2257−2261.
(26) The LACV3P basis set is a triple-ζ contraction of the LACVP basis set developed and tested at Schrödinger, Inc.[27]
(27) *Jaguar 5.5*; Schrödinger, Inc.: Portland, OR, 2003.
(28) Perdew, J. P. *Phys. Rev. B* **1986**, *33*, 8822.
(29) Lynch, B. J.; Fast, P. L.; Harris, M.; Truhlar, D. G. *J. Phys. Chem. A* **2000**, *104*, 4811−4815.

done also at the QM/MM level using another functional, as described below. Detailed comments about the accuracy of UB3LYP for the problem at hand appear in the SI document. Frequency calculations and zero-point energy corrections were performed with the GAUSSIAN 98 and 03 packages.[30]

B. QM/MM Methodology and Software. The QM/MM method[31] dissects the total enzyme into two subsystems: the active center and the rest. The active center is described by a QM method, in the present case DFT in the unrestricted Kohn−Sham formalism employing the UB3LYP functional. The rest of the system (see below) is treated by molecular mechanics using a force field calibrated for proteins.[32] The two subsystems are allowed to interact by electrostatic and van der Waals terms, such that the QM subsystem adapts its electronic structure and charge distribution to the field exerted by the protein environment. In the present study, we apply the electrostatic embedding scheme[33] that incorporates the MM charges into the one-electron Hamiltonian of the QM procedure, while the dangling bonds at the QM/MM boundary are capped with hydrogen link atoms[34] in the framework of the charge shift method. The Chemshell software[35] is used to perform the QM/MM calculations by integrating the TURBOMOLE package[36] for QM and the DL-POLY program[37] for MM using the CHARMM22 force field.[32]

To be consistent with a recent QM/MM study of Cpd I of HRP,[38] we used here two basis sets for the QM/MM calculations: for geometry optimization we utilized B1, i.e., LACVP that was described above, and for single-point energy calculations we used the larger all electron basis set, B3. In B3, iron is described by use of a Wachters all-electron basis set augmented with diffuse d and f polarization functions,[39] while the immediate coordination sphere of iron and other electronegative atoms are represented by 6-31+G(d), and the remaining atoms are represented by 6-31G(d). These single-point energies are labeled as B3//B1.

To ascertain the validity of UB3LYP, single points with B3 were also run with the UPBE0 functional,[40] which has been shown to perform like SORCI and CASPT2 for discriminating spin states in iron(II) complexes.[41] Data are given in the SI (Table S23) and are very similar to those obtained with UB3LYP.

Scheme 3. QM Model I and QM Model II

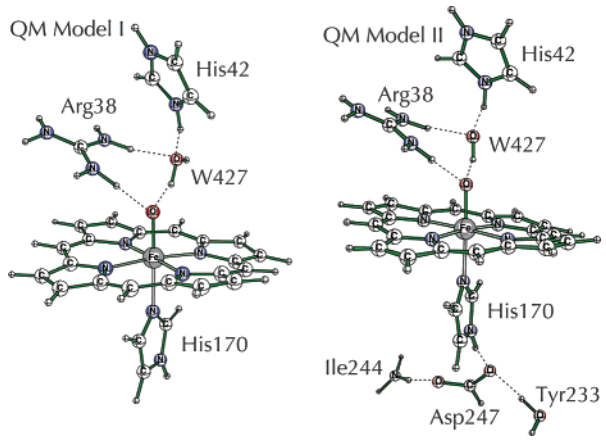

C. Setup of the System. To prepare suitable initial structures for the QM/MM calculations, we started from the experimental X-ray structure of HRP Cpd I (PDB code 1HCH)[10] and built a complete model of the solvated enzyme by adding the missing hydrogen atoms and a 16-Å-thick water solvent layer. The total charge of the so-generated system was 1+, corresponding to the following protonated states of the various residues: aspartates (Asp) and glutamates (Glu) are negatively charged (Asp 8, 20, 29, 43, 50, 56, 66, 81, 99, 125, 132, 150, 162, 182, 194, 220, 222, 230, 247, 258, 282; Glu 25, 64, 88, 238, 239, 249, 279), and arginines (Arg) and lysines (Lys) are positively charged (Arg 19, 27, 31, 38, 62, 75, 82, 93, 118, 123, 124, 153, 159, 178, 183, 206, 224, 264, 283, 298, 302; Lys 65, 84, 149, 174, 232, 241). One more positive charge is "located" on the heme moiety. The histidines His 40 and His 170 were singly protonated and hence electrically neutral. We chose to doubly protonate His 42 in order to transfer the second proton to the Fe═O moiety, thus generating Fe−OH. This should not be considered as a static representation of the situation of His 42, but rather as a dynamic state that corresponds either to an acidic pH, in which a proton is taken from the surrounding solvent and is transferred to the heme, or to a case where the proton released from initial substrate oxidation (Scheme 1) resides momentarily on His 42, only to be transferred to the Fe═O moiety of **2a**. The complete system consists of 19 452 atoms, including 13 395 atoms in the solvent. The system was subsequently relaxed by performing pure force field energy minimizations and short molecular dynamics (MD) simulations, using the CHARMM22 force field. During these classical force field calculations, the coordinates of the entire heme unit and the coordinated histidine were kept fixed. The MD calculations did not significantly modify the structure compared with the initial X-ray structure. Therefore, we performed the QM/MM calculations on the coordinates obtained after simple force field energy minimizations and short MD on the inner solvent layer (in order to remove close contacts).

D. QM and QM/MM Regions. Two types of QM subsystem were investigated by QM/MM calculations and are shown schematically in Scheme 3 using the oxo-ferryl isomer. Both

(30) (a) Frisch, M. J.; et al. *Gaussian 98*, Revision A.07; Gaussian, Inc.: Pittsburgh, PA, 1998. (b) Frisch, M. J.; et al. *Gaussian 03*, Revision B.05; Gaussian, Inc.: Pittsburgh, PA, 2003.
(31) For a small selection of reviews, see: (a) Aqvist, J.; Warshel, *A. Chem. Rev.* **1993**, *93*, 2523−2544. (b) Gao, J. In *Reviews in Computational Chemistry*; Lipkowitz, K. B., Boyd, D. B., Eds.; VCH: Weinheim, 1995; Vol. 7, p 119. (c) Mordasini, T. Z.; Thiel, W. *Chimia* **1998**, *52*, 288−291. (d) Monard, G.; Merz, K. M., Jr. *Acc. Chem. Res.* **1999**, *32*, 904−911. (e) Sherwood, P. In *Modern Methods and Algorithms of Quantum Chemistry*; Grotendorst, J., Ed.; NIC Series 3; John von Neumann Institute for Computing: Jülich, 2000; p 285. (f) Gao, J.; Truhlar, D. G. *Annu. Rev. Phys. Chem.* **2002**, *53*, 467−505. (g) Field, M. J. *J. Comput. Chem.* **2002**, *23*, 48−58. (h) Monard, G.; Prat-Resina, X.; Gonzalez-Lafont, A.; Lluch, J. M. *Int. J. Quantum Chem.* **2003**, *93*, 229−244. (i) Ridder, L.; Mulholland, A. *Curr. Top. Med. Chem.* **2003**, *3*, 1241−1256.
(32) MacKerell, A. D., Jr.; et al. *J. Phys. Chem. B* **1998**, *102*, 3586−3616.
(33) Bakowies, D.; Thiel, W. *J. Phys. Chem.* **1996**, *100*, 10580−10594.
(34) (a) Field, M. J.; Bash, P. A.; Karplus, M. *J. Comput. Chem.* **1990**, *11*, 700−733. (b) Amara, P.; Field, M. J. *Theor. Chem. Acc.* **2003**, *109*, 43−52. (c) Reuter, N.; Dejaegere, A.; Maigret, B.; Karplus, M. *J. Phys. Chem. A* **2000**, *104*, 1720−1735. (d) Singh, U. C.; Kollman, P. A. *J. Comput. Chem.* **1986**, *7*, 718−730. (e) Derat, E.; Bouquant, J.; Humbel, S. *J. Mol. Struct. (THEOCHEM)* **2003**, *632*, 61−69. (f) de Vries, A. H.; Sherwood, P.; Collins, S. J.; Rigby, A. M.; Rigutto, M.; Kramer, G. J. *J. Phys. Chem. B* **1999**, *103*, 6133−6141.
(35) Sherwood, P.; et al. *J. Mol. Struct. (THEOCHEM)* **2003**, *632*, 1−28.
(36) Ahlrichs, R.; Bär, M.; Häser, M.; Horn, H.; Kölmel, C. *Chem. Phys. Lett.* **1989**, *162*, 165−169.
(37) Smith, W.; Forester, T. *J. Mol. Graph.* **1996**, *14*, 136−141.
(38) Derat, E.; Cohen, S.; Shaik, S.; Altun, A.; Thiel, W. *J. Am. Chem. Soc.* **2005**, *127*, 13611−13621.
(39) Wachters, A. J. H. *J. Chem. Phys.* **1970**, *52*, 1033−1036.
(40) (a) Perdew, J. P.; Burke, K.; Ernzerhof, M. *Phys. Rev. Lett.* **1996**, *77*, 3865−3868. (b) Perdew, J. P.; Ernzerhof, M.; Burke, K. *J. Chem. Phys.* **1996**, *105*, 9982−9985.
(41) Fouqueau, A.; Casida, M.; Daku, L. M. L.; Hauser, A.; Neese, F. *J. Chem. Phys.* **2005**, *122*, 044110−13.

models involve the distal residues Arg_{38} and His_{42} that were shown to be crucial for reproducing the Mössbauer properties of Cpd I.[38] As such, the first model (QM Model I) includes the heme (and its proximal His_{170} ligand represented by an imidazole), Arg_{38}, His_{42}, and a bridging water (W_{427}). The second model (QM Model II) adds to the previous one three proximal residues, the aspartic acid hydrogen-bonded to the imidazole (Asp_{247}) and the counterions of this aspartic acid (Tyr_{233} and Ile_{244}). As was done previously for this model, here, too, the Tyr_{233} is modeled as an OH group only and the dangling bond is saturated with a hydrogen link atom (H), thus leading to H_2O; Ile_{244} is modeled as $NH_2(H)$, which represents the part of the backbone of this residue that is hydrogen-bonded to the Asp_{247}.

Finally, during the QM/MM calculations, the region that undergoes QM/MM optimization involved, as in previous work reported by this group,[38] the following residues, in addition to the QM models in Scheme 3: Arg_{31}, Ser_{35}, Arg_{38}, Phe_{41}, His_{42}, Ser_{73}, Leu_{138}, Pro_{139}, Ala_{140}, Pro_{141}, Ser_{167}, His_{170}, Gln_{176}, Ile_{244}, Asp_{247}, Phe_{221}, Tyr_{233}, W_{427}, W_{423}, and W_{278}.

E. Mössbauer Parameters. Since Mössbauer spectra are available in the literature, it is possible to compare Mössbauer parameters obtained by theoretical means with the experimental values and to use the calculated values for the yet-unobserved electromers and tautomers, hopefully as means of clear-cut identification of the experimentally detectable species. Using the ORCA program,[42] the Mössbauer parameters were obtained from single-point UB3LYP calculations (at the geometries obtained after QM/MM optimization). The isomer shift was evaluated from the electron density at the iron nucleus.[43] Iron was described by the triply polarized core properties basis set CP(PPP),[43] and the other atoms were described by the SV(P) basis set[44] with the inner s-functions left uncontracted. For the iron atom, an enhanced integration grid was used, and the overall integration accuracy was increased to 7.[43] MM point charges were included in these calculations to probe the effect of the protein environment. The Mössbauer parameters were calculated for all the forms of HRP Cpd II.

Results

All the results are collected in the SI document; herein we present key data.

QM Studies: Geometric and Electronic Structures of the 2a and 2b Forms of Cpd II. The key geometric features of the various forms of Cpd II are shown in Figure 1, where the various labels follow Scheme 2. In addition, near each structure we indicate the spin quantum number, *S*, that is either 1 (triplet) or zero (singlet), and the major group spin densities, ρ; a positive group spin density means that the group is populated by excess spin-up (α) electrons, whereas a negative group spin density corresponds to an excess of spin-down (β) electrons on the respective group. In all cases, the singlet states were calculated as the broken-symmetry open-shell states. The relative energies of the spin states and electromeric forms are given in Table 1.

A few main features are apparent in Figure 1: (a) The oxo-ferryl isomer has the shortest Fe−O bond, almost 0.1 Å shorter than in the hydroxo-ferryl electromer, **2b**(Fe^{IV}). (b) The form with the longest Fe−O bond is the **2b**(Fe^{III}) electromer of the hydroxo-ferryl isomer. (c) For the isomers **2a** and **2b**(Fe^{IV}), the Fe−O(H) bond is longer for the singlet states, while for **2b**(Fe^{III}) the two spin states have precisely the same Fe−OH bond lengths, albeit they differ marginally in the Fe−N_{His} bond length. (d) In accord with a previous study,[6c] the conformations of the **2b**(Fe^{IV}) and **2b**(Fe^{III}) electromers of the hydroxo-ferryl isomer are different; **2b**(Fe^{IV}) prefers a dihedral angle of 90° (between the imidazole and FeOH planes), while the **2b**(Fe^{III}) electromer prefers a dihedral angle of 0°. (e) In the **2a** isomer, the spin density is almost equally partitioned between the iron and the oxygen group, while in the **2b** isomer most of the spin is on the iron for the **2b**(Fe^{IV}) electromer and on the iron and porphyrin in the **2b**(Fe^{III}) electromer.

The data in Table 1 show that the ground states of **2a** and **2b**(Fe^{IV}) are the corresponding triplet states, whereas the two spin states of **2b**(Fe^{III}) are virtually degenerate. In addition, the most stable electromer among the hydroxo-ferryl forms is **2b**(Fe^{III}), for which both the singlet and the triplet states are considerably more stable than the triplet state of **2b**(Fe^{IV}). For obvious reasons, a comparison of the relative stability of the oxo-ferryl and hydroxo-ferryl forms, **2a** vs **2b**, at the QM-only level could not be made. All three functionals used in the study gave the same qualitative trends. As will be seen later, this result recurs with QM(UB3LYP)/MM and QM(UPBE0)/MM. This uniform trend is reassuring regarding the use of B3LYP for this problem.

Most of the above trends for **2a** and **2b** can be understood by considering the electronic structures of the species in Scheme 2. For **2a** and **2b**(Fe^{IV}), the two π^* orbitals that have significant iron d-character contributions are singly occupied, and therefore the d−d exchange favors the triplet states by considerable margins. On the other hand, the spin states of **2b**(Fe^{III}) are almost degenerate since one electron occupies a π^*(FeO) orbital, while the other occupies an a_{2u}(Por) orbital, which are spatially distant and maintain a very small exchange interaction. In fact, these states are analogous to the degenerate states of Cpd I of HRP[38] and other Cpd I species.[4,45] As depicted in Figure 2, the calculations further show that the electronic structure of the lowest energy for **2b**(Fe^{III}) involves double occupancy in the π^*_{xz} orbital, which is dominantly an iron d-orbital, while the single occupancy is in the π^*_{yz} orbital that has a strong antibonding character across the Fe−OH bond. The configuration with the $\pi^*_{xz}{}^1\pi^*_{yz}{}^2$ orbital occupation is an excited state about 10 kcal/mol above the ground state. The same finding was reported for the corresponding **2b**(Fe^{III}) electromer of the hydroxo-ferryl isomer in the P450 enzyme.[46]

A feature that differs for the P450 and the HRP enzymes is the relative stability of **2b**(Fe^{IV}) and **2b**(Fe^{III}). In cytochrome P450 (and in its chloroperoxidase analogue[8b]), the most stable hydroxo-ferryl electromer in the gas phase is **2b**(Fe^{IV}), while polarity and NH- - -S hydrogen-bonding effects are required to make the **2b**(Fe^{III}) slightly more stable.[46] By contrast, here in HRP, **2b**(Fe^{III}) is significantly more stable than **2b**(Fe^{IV}) already in the gas phase, and as will be seen immediately, the protein environment further prefers the Fe^{III} electromer.

QM/MM Studies of the 2a and 2b Forms of Cpd II. Figure 3 shows the optimized QM(UB3LYP/B1)/MM(CHARMM)

(42) Neese, F. *ORCA*, Version 2.4, Revision 10; Max-Planck-Institut für Bioanorganische Chemie: Mülheim a.d. Ruhr, Germany, 2004.
(43) Neese, F. *Inorg. Chim. Acta* **2002**, *337*, 181−192.
(44) Schäfer, A.; Horn, H.; Ahlrichs, R. *J. Chem. Phys.* **1992**, *97*, 2571−2577.
(45) Shaik, S.; Kumar, D.; de Visser, S. P.; Altun, A.; Thiel, W. *Chem. Rev.* **2005**, *105*, 2279−2328.
(46) (a) See ref 6c. (b) Schöneboom, J. C.; Cohen, S.; Lin, H.; Shaik, S.; Thiel, W. *J. Am. Chem. Soc.* **2004**, *126*, 4017−4034. (c) See ref 6d.

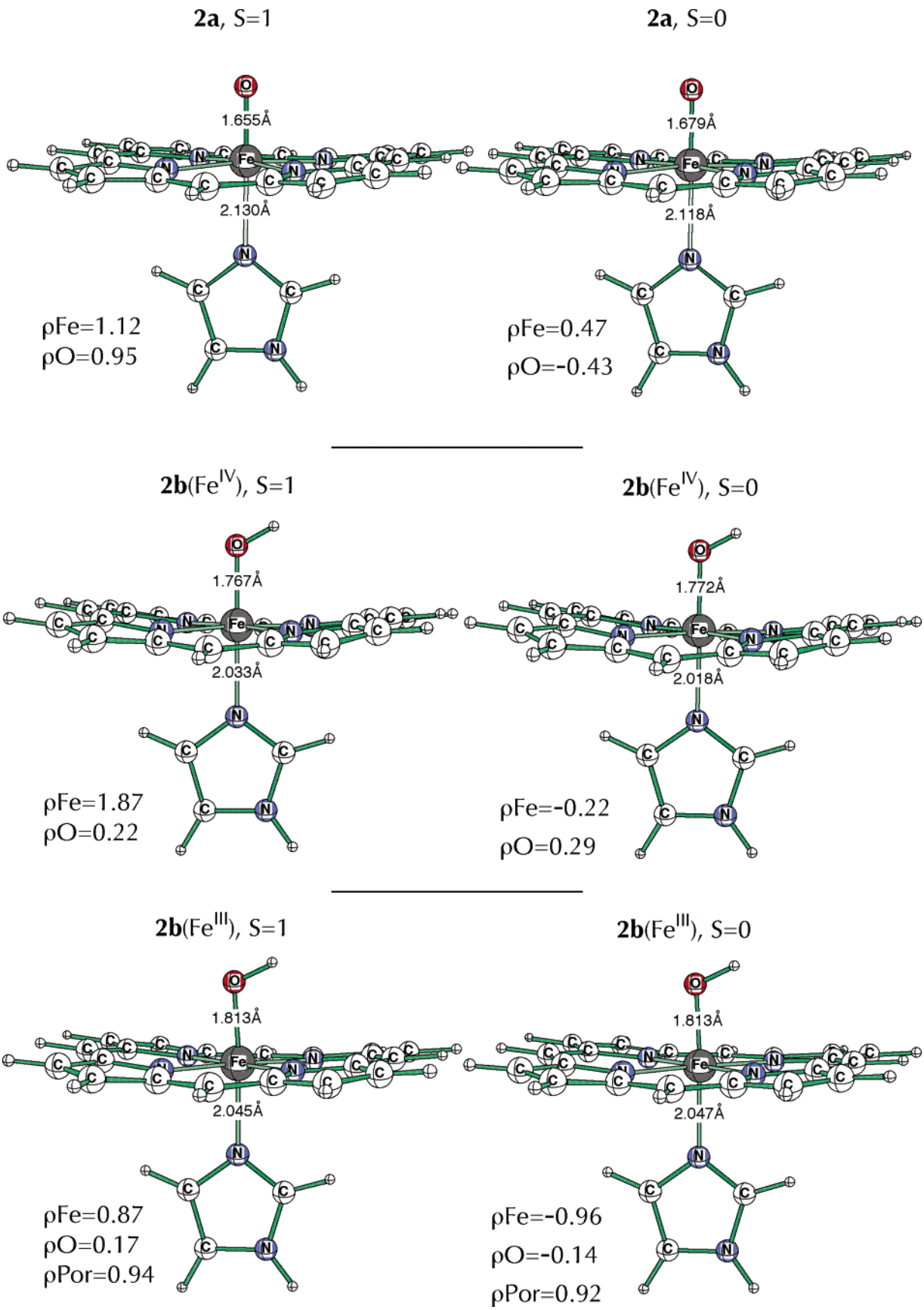

Figure 1. Key UB3LYP/B1 geometric features, spin quantum numbers (S), and major spin density (ρ) values (B2//B1) for the **2a** and **2b** forms of Cpd II of HRP.

structures and spin densities for QM Model I, with Arg_{38}, His_{42}, and W_{427} interacting with the oxo- and hydroxo-ferryl moieties by hydrogen-bonding and electrostatic interactions. Figure 4 shows the same data for QM Model II. Table 2 summarizes the

Table 1. QM Energetic Data (in kcal/mol) for the Electromers and Tautomers of the Bare Cpd II Species of HRP with Different Functionals

		UB3LYP			UB3P86[b]	UMPW1K	
Cpd II species/spin	state	ΔE(B1)[a]	$\Delta(E+\text{ZPC})$[a]	ΔE(B2//B1)[b]	ΔE(B1)[a]	ΔE(B1)[a]	ΔE(B2//B1)[b]
2a/triplet	$\pi^*\pi^*$	0.00	0.00	0.00	0.00	0.00	0.00
2a/singlet	$\pi^*\pi^*$	9.21	8.82	9.72	9.34	8.10	n.c.[c]
2b(Fe^{IV})/triplet	$\pi^*\pi^*$	0.00	0.00	0.00	0.00	0.00	0.00
2b(Fe^{IV})/singlet	$\pi^*\pi^*$	10.36	8.64	11.44	10.70	14.91	16.53
2b(Fe^{III})/triplet	π^*a_{2u}	−5.35	−6.26	−3.48	−1.72	−13.13	−9.07
2b(Fe^{III})/singlet	π^*a_{2u}	−5.34	−6.26	−3.51	−1.60	−13.34	−9.42

[a] B1 is the LACVP basis set. [b] B2 is the LACV3P+* basis set. B2//B1 corresponds to energy calculations obtained with the UB3LYP/B1 geometry. [c] Not converged.

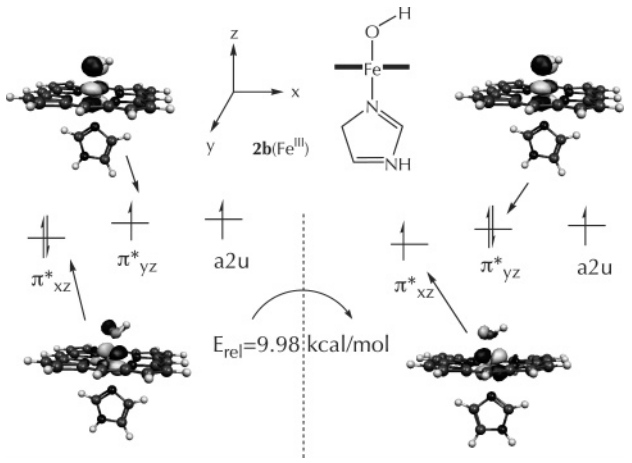

Figure 2. Comparison of the ground and excited triplet states for **2b**(Fe^{III}). The $\pi^*_{xz}{}^1\ a_{2u}{}^1$ state corresponds to a vertical excited state of the $\pi^*_{yz}{}^1\ a_{2u}{}^1$ state.

relative energies and the transition states for protonation of **2a** and its conversion to **2b**. Figures 5 and 6 show the energy profile and transition-state structures for this conversion.

QM/MM Structures and Spin Densities of the 2a and 2b Forms. Inspection of Figures 3 and 4 reveals a few major trends. First, it is apparent that the addition of the proximal residues in QM Model II in Figure 4 has little effect on the geometry and spin density of all the isomers of Cpd II; hence, the smaller Model I is appropriate for investigating Cpd II of HRP. Second, compared with the gas-phase structures in Figure 1, the QM/MM structures in Figures 3 and 4 have longer Fe−O bonds and shorter Fe−N_{Im} bonds. Thus, the interactions of the Fe−O(H) moiety with the protein residues exert the well-known trans effect[47] on the N_{Im}−Fe−O moiety. Second, for **2a**, the hydrogen-bonding interaction causes a significant spin density shift from the oxygen of the oxo group to the iron. Thus, while in the gas phase (Figure 1), the spin distribution in the Fe═O moiety is almost 1:1, each atom carrying one spin, whereas in the protein environment, most of the spin density, ca. 1.7, is on the iron and a small fraction, ca. 0.4, is on the oxygen. The same observations, Fe−O bond lengthening and spin density shift from oxo to iron, were noted previously for Cpd I of HRP[38] and for Cpd II of myoglobin.[11b] For HRP Cpd I, these effects were essential for reproducing the observed Mössbauer parameters for Cpd I and hence are deemed essential also in the present study of Cpd II. These effects were explained before[38] using a valence bond (VB) mixing diagram showing how *the strong hydrogen-bonding with the Fe═O moiety converts the Fe═O π-bonding from a covalent bond, with spin density of unity on each of the Fe and O atoms, to a more ionic bond* by mixing in an ionic structure that has two unpaired electrons on Fe and none on O. The net result of this ionic mixing is an increase of the spin density on iron to a value close to 2 and the concomitant decrease on oxygen to a value smaller than 0.5. The same admixture of the ionic structure into the covalent structure causes elongation of the Fe−O bond and a trans effect along the N_{ImH}−Fe−O axis. These considerations apply here to the oxo-ferryl isomer, **2a**, of Cpd II. Finally, the structural parameters of **2b**(Fe^{IV}) in Figures 3 and 4 are very close to the X-ray crystallographic data reported by Berglund et al.[10] By contrast, the only geometric characteristics that may correspond to the apparently conflicting EXAFS data[8,9] are those for **2a** and **2b**(Fe^{III}), where the Fe−O distances are 1.716 and 1.870−1.872 Å, respectively. Still, the fact that none of these isomers reveals an overly long Fe−O distance of 1.92 Å, as reported in ref 9, suggests that the latter datum may correspond to a new species that is discussed later.

QM/MM Relative Energies of the 2a and 2b Forms and Their Interconversion Barriers. Table 2 shows the relative QM/MM energies for all the forms with the two models and two basis sets. It is seen that, in both models and the two basis sets, the most stable forms are **2b**; the more stable electromer is **2b**(Fe^{III}), with the singlet state being very slightly more stable than the triplet state. The only datum that exhibits a basis set effect is the energy of **2b**(Fe^{IV}) relative to **2a**: with B1, **2b**(Fe^{IV}) is more stable by 3.3−3.6 kcal/mol, while with B3, the relative stability increases to 9.8−10.7 kcal/mol. We verified that virtually the entire change occurs in the QM energy part of the QM/MM energy (see Tables S10 and S16 in the SI). Inspection of the charges of the species show that, as one changes from B1 to B3, the charge on the oxygen atom of **2a** becomes significantly less negative (−0.60 to −0.18), while for **2b**(Fe^{IV}) the group charge on the OH groups becomes positive (−0.16 to +0.25) due to the increased positive charge on H; thus, the increased positive charge of the proton of the hydroxyl group with B3 is responsible for a stronger hydrogen-bonding interaction with W_{427} and for the increased stabilization of **2b**(Fe^{IV}) relative to **2a**. Finally, it is important to emphasize once again that the **2b**(Fe^{III}) electromer is more stable than **2b**(Fe^{IV}) both in the protein and in the gas phase (Tables 2 vs 1) by a significant amount, 3.5−6 kcal/mol, whereas in cytochrome P450, there is only a slight preference for **2b**(Fe^{III}) in the protein environment.[46] The same qualitative trends and quantitative relations were obtained with QM(UPBE0)/MM calculations (see

(47) (a) Hartley, F. R. *Chem. Soc. Rev.* **1973**, *2*, 163−179. (b) Weinhold, F.; Landis, C. R. *Valency and Bonding*; Cambridge University Press: Cambridge, England, 2005; pp 473−474. (c) Marti, M. A.; Scherlis, D. A.; Doctorvitch, F. A.; Ordejon, P.; Estrin, D. A. *J. Biol. Inorg. Chem.* **2003**, *8*, 595−600.

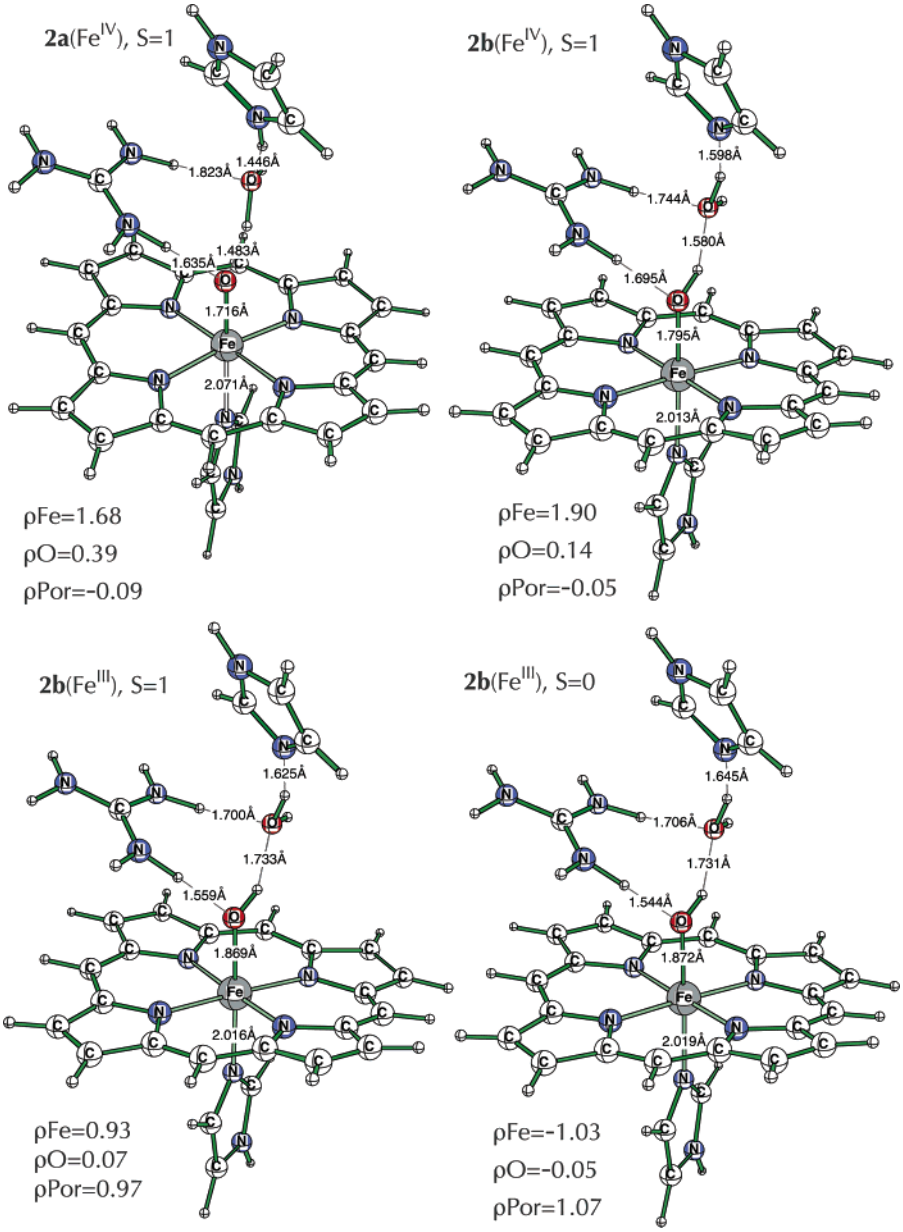

Figure 3. Key QM(UB3LYP/B1)/MM(CHARMM) geometric features, spin quantum numbers (S), and major spin density (ρ) values (B2//B1) for the **2a** and **2b** forms of Cpd II of HRP, QM Model I.

Table S24 in the SI). Thus, in the sense that UPBE0 is considered to be accurate for spin states of iron,[41] and that all the results are reproduced at whichever level we used, we deem the conclusions to be reliable.

Figures 3 and 4 show that the crystal water molecule W_{427} is ideally positioned to shuttle a proton from the protonated His_{42} to the oxygen atom of the oxo-ferryl group of **2a** and to form, thereby, **2b**. Indeed, we could easily find a mechanism leading from **2a** to **2b**(Fe^{IV}). However, all our attempts to connect from of **2a** to **2b**(Fe^{III}), or vice versa starting from **2b**(Fe^{III}) toward **2a**, were unsuccessful and led to a doubly protonated Cpd II structure, the "surprise" species that is discussed in the next section (see Figure 7). Accordingly, Table 2 includes the energy of the transition state for the protonation of **2a** to **2b**(Fe^{IV}), **TS**(**2a** → **2b**(Fe^{IV})), while Figure 5 depicts the energy profile for this transformation and Figure 6 shows the structures of these transition states for Models I and II. It is seen from Table 2 and Figure 5 that the transformation of **2a** to **2b**(Fe^{IV}) involves a tiny barrier of 1.6−1.7 kcal/mol, and the transition states in Figure 6 show that the proton is shuttled via the intervening W_{427} molecule. Thus, in principle, the oxo-ferryl and hydroxo-ferryl species are genuine minima separated by a tiny barrier. Furthermore, in the absence of W_{427}, the distance from His_{42} to the oxo-ferryl would be too long, and the barrier will be much higher.

Appearance of New Isomers during the Attempts To Convert 2a to 2b(Fe^{III}). As already noted, we could not transform **2a** to **2b**(Fe^{III}). We tried, however, to start from the singlet and triplet states of **2b**(Fe^{III}) and deprotonate them to obtain the corresponding states of **2a**. This process resulted, however, in an additional protonation of **2b**(Fe^{III}) by Arg_{38}, to yield the corresponding states of **2b-H**$^+$(Fe^{III}) isomers described in Figure 7. The barriers for these processes can be estimated from the energy scans as ca. 6 kcal/mol for the two spin states (see Figure S4 in the SI). These new isomers are ferric-aqua complexes that involve a porphyrin radical-cationic state, i.e.,

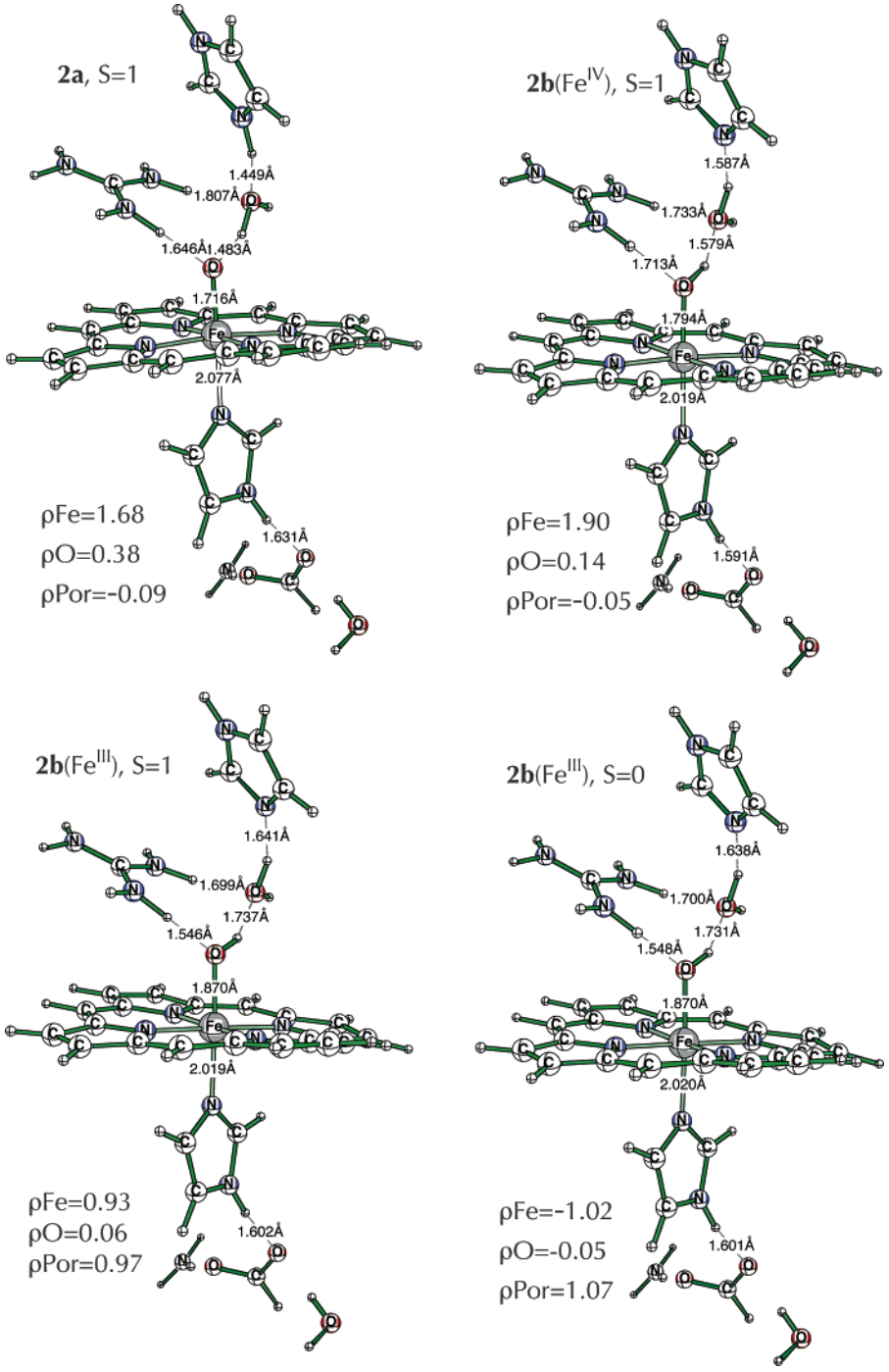

Figure 4. Key QM(UB3LYP/B1)/MM(CHARMM) geometric features, spin quantum numbers (S), and major spin density (ρ) values (B2//B1) for the **2a** and **2b** forms of Cpd II of HRP, QM Model II.

$[ImPor^{+\bullet}Fe^{III}(OH_2)]^{2+}$, having the same electronic structures as the two spin states of **2b**(Fe^{III}), and are therefore potentially additional isomers of Cpd II HRP, with similar oxidative capability due to the high-valence iron ion. The **2b-H**$^+$(Fe^{III}) species are, for singlet/triplet, 9.2/9.0 (with B1//B1) and 16.2/16.2 (with B3//B1) kcal/mol more stable than the triplet-state **2a** isomer and 1.8/2.0 (B1//B1) and 0.7/0.7 (B3/B1) kcal/mol higher than the singlet **2b**(Fe^{III}) form. We note that the Fe−O bond length in the **2b-H**$^+$(Fe^{III}) species is 1.92 Å, identical, and perhaps accidentally so, to one of the EXAFS results.[9] The appearance of the "surprise" species may look suspicious since Arg has a large pK_a (11−12) and after protonation it remains in its conjugated base form. Thus, while this may suggest that the "surprise" species is possibly a computational artifact, as we already emphasized, the deprotonated Arg_{38} residue is not a static situation but rather a short-lived state, since protons can be shuttled from the surface to reprotonate Arg_{38}. Another interesting point is that *there is no significant barrier for the formation of* ***2b****(*Fe^{III}*-H)*; this, as well as the unusual derivation of these species from **2b**(Fe^{III}), requires some rationale.

Mössbauer Parameters for the Isomers of Cpd II of HRP. The isomer shifts, quadrupole splittings, and asymmetry parameters for all the isomers of Cpd II of HRP, using QM Model I, are given in Table 3, alongside the corresponding experimental data.[22] The calculated quadrupole splittings, isomer shifts, and asymmetry parameters match the experimental data for only one

Table 2. QM(UB3LYP)/MM(CHARMM) Relative Energy (kcal/mol) Data for the Various Isomers of Cpd II of HRP, and the Transition State for Protonation of **2a**, for Two QM Models, I and II, with Basis Sets B1 and B3[a]

		model I		model II	
compound	state	B1	B3//B1	B1	B3//B1
2a/triplet	$\pi^*\pi^*$	0.00	0.00	0.00	0.00
transition state	$\pi^*\pi^*$	0.71	1.59	0.74	1.67
2b(Fe^{IV})/triplet	$\pi^*\pi^*$	−3.60	−10.67	−3.29	−9.83
2b(Fe^{III})/singlet	π^*a_{2u}	−11.04	−16.97	−10.58	−16.09
2b(Fe^{III})/triplet	π^*a_{2u}	−10.65	−15.60	−10.38	−15.83

[a] Model I includes only distal residues (Scheme 3, Figure 3), while Model II includes also proximal residues (Scheme 3, Figure 4). B1 is LACVP, and B3 involves on Fe Wachters (2d,f) and 6-31+G(d) on all the first coordination shell of iron, 6-31G(d) on the rest of the atoms.

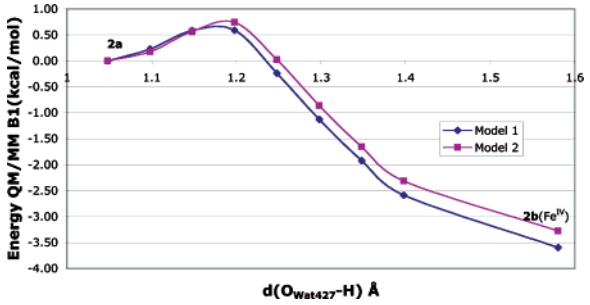

Figure 5. QM(UB3LYP/B1)/MM(CHARMM) energy scans for the conversion of **2a** and **2b**(Fe^{IV}) by protonation via the His_{42}—H^+- - -W_{427} channel. Shown are the profiles for QM Models I and II.

isomer, the oxo-ferryl isomer **2a**. The calculated data for all other isomers are sufficiently different to rule out the possibility that the isomers **2b** and its two electromers were ever observed in the Mössbauer experiment. Since **2b** was observed at least by two other techniques (X-ray and EXAFS), it is clear that the Mössbauer study has missed the various **2b** isomers. As the formation of the latter species involves acidic pH and requires proton transfer mediated by W_{427} inside the active site, perhaps the omission is rooted in the preparation of Cpd II for the Mössbauer spectroscopy or in the low temperature usually used to record the spectra.

Discussion

The foregoing results show that QM/MM calculations reproduce the structural and spectral features that have been observed for Cpd II species of HRP. However, the calculations describe additional features and reveal six low-lying isomers that are placed on an energy scale in Figure 8 (see also QM(UPBE0)/MM in Table S24 in the SI). Only two of these, the two least stable isomers, the oxo-ferryl, **2a**, and hydroxo-ferryl, **2b**(Fe^{IV}), have so far been observed or probed by experimental techniques.[8,10,13,16,19] The other four isomers, **2b**(Fe^{III}) and **2b-H**$^+$-(Fe^{III}) in two spin states, $S = 0$ and 1, have never been reported/discussed for HRP or for any other heme enzyme. Furthermore, Cpd II has never been formulated before as a ferric-aqua porphyrin radical-cation complex as the **2b-H**$^+$(Fe^{III}) species. That these missing isomers are not merely figments of theory is suggested by the facts that (i) a species of the **2b**(Fe^{III}) type has been reported before in synthetic heme complexes,[6a] (ii) the methods used to assign Fe^{IV} or Fe^{III} were not really conclusive to exclude one of the possibilities,[11b] and (iii) the Mössbauer method that can distinguish these oxidation states[22] has altogether missed the **2b**-type isomers.[13] Based on these considerations and the fact that the missing isomers were revealed in the present study by various theoretical methods, the most practical approach is to assume that they exist and to seek a general understanding of the picture.

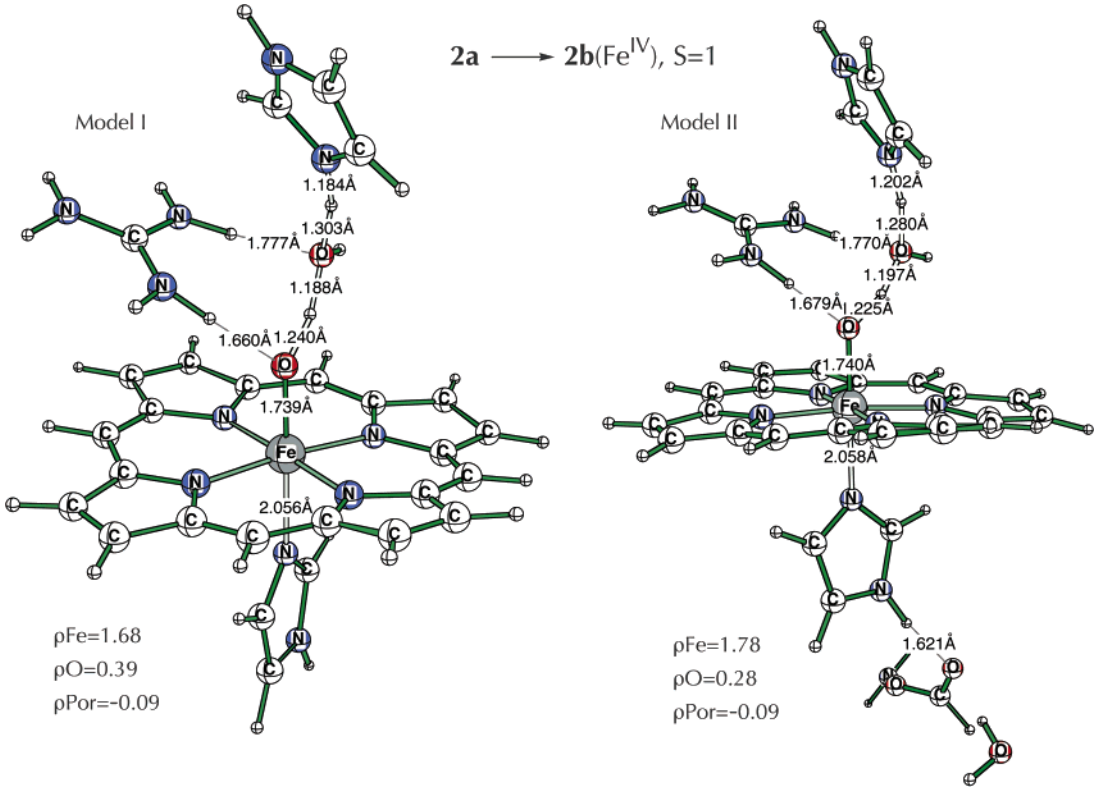

Figure 6. QM(UB3LYP/B1)/MM(CHARMM) optimized transition-state structures for the conversion of **2a** to **2b**(Fe^{IV}) in QM Models I and II.

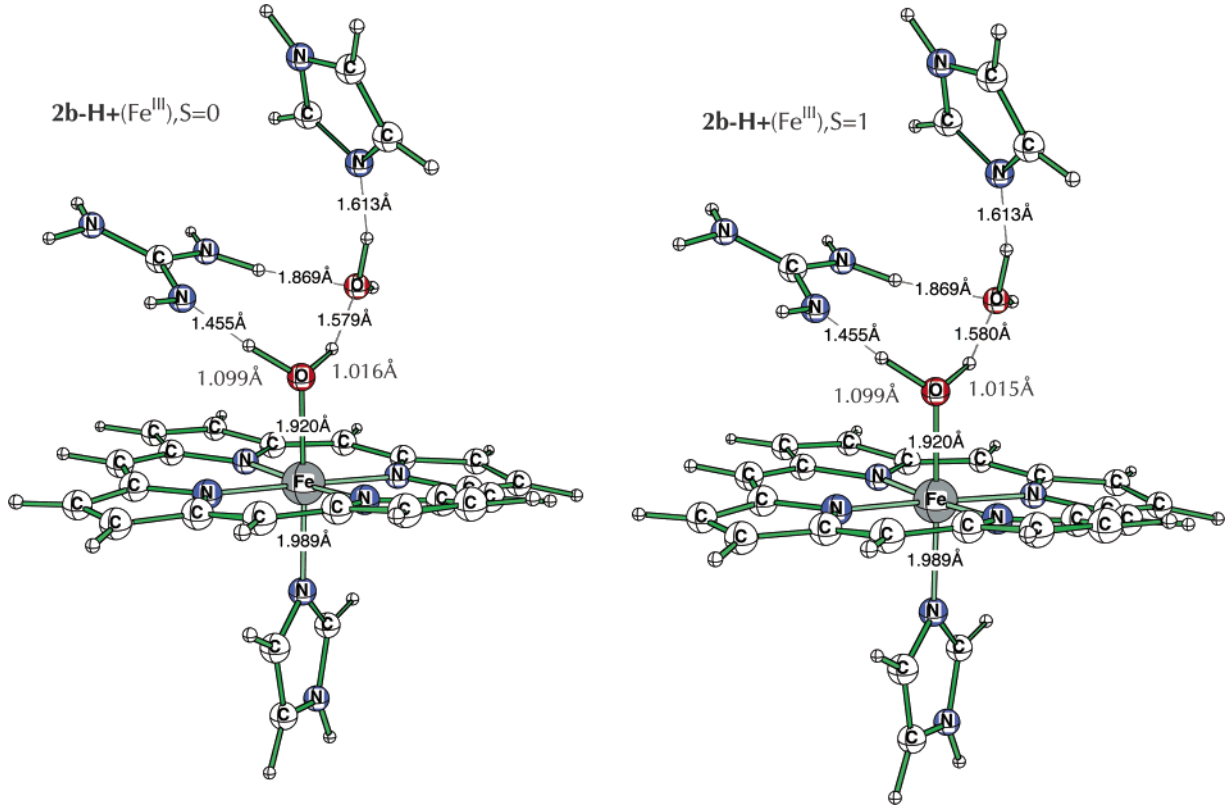

Figure 7. Optimized QM/MM structures of the singlet (left-hand side)/triplet (right-hand side) states of **2b-H**$^+$(Fe^{III}) obtained by an energy scan starting from the minimum found for the singlet/triplet **2b**(Fe^{III}) state with the O(W_{427})−H hydrogen bond (see Figure S4 in the SI) and trying to transfer the proton from the hydroxo group to W_{427} and then back to His_{42}. This attempt resulted in a proton abstraction from Arg_{38} and the formation of the **2b-H**$^+$(Fe^{III}) species (their total charge is 2+).

Table 3. Experimental and Calculated Mössbauer Isomer Shifts, δ(^{57}Fe) (mm/s), Quadrupole Splittings, ΔE_Q (mm/s), and Asymmetry Parameters, η, for Cpd II of HRP

compound/state	η	ΔE_Q	δ
experimental data	0	1.61	0.03
2b(Fe^{III})/triplet	0.437	−2.322	0.31
2a/triplet	0.07	1.717	0.01
2b(Fe^{IV})/triplet	0.064	2.428	0.00
2b-H$^+$(Fe^{III})/triplet	0.132	−2.595	0.30

Our discussion will attempt to draw the relationships among these species and answer the following questions: (a) Why is **2b**(Fe^{III}) the most stable electromer of HRP Cpd II, whereas in P450, **2b**(Fe^{IV}) is almost as stable as **2b**(Fe^{III}) if not more so?[8b,46] (b) What might be the reason that **2b**(Fe^{III}) cannot be obtained directly by protonating **2a**, and what is then the origin of **2b-H**$^+$(Fe^{III})? (c) What might be the reason that **2b**(Fe^{III}) and **2b-H**$^+$(Fe^{III}) species have never been reported? (d) If the protonation barrier that converts **2a** to yield **2b**(Fe^{IV}) is so small (Figure 5), why does **2a** exist at all and can it even be probed experimentally? (e) Since there are two different spin states among the forms of Cpd II, what kind of reactivity scenarios are expected for these species?

On the Relative Stability of the Isomers of Cpd II of HRP Vis-à-Vis P450. We recall that in P450, the isomer **2b**(Fe^{III}) is higher in energy than **2b**(Fe^{IV}), and only with the addition of bulk polarity and hydrogen bonding interactions of the enzyme, does the former isomer become more stable than the latter.[46] By contrast, the **2b**(Fe^{III}) isomer of HRP (see Table 1) is lower in energy than **2b**(Fe^{IV}), already in the isolated-molecule level, and the energy difference gets larger, ca. 6 kcal/mol, in the protein environment. This difference is rooted in the different electronic characters of the proximal ligands, as discussed at length before.[48] We recall that the sulfur orbitals mix strongly with the heme orbitals (the d-orbitals of iron and the a_{2u} orbital of the porphyrin); these orbitals acquire, thereby, strong antibonding character and are consequently raised in energy (the effect is also called the "push effect" [1d,e,16]). By contrast, the imidazole orbitals mix with the heme orbitals to a lesser extent, very slightly with a_{2u} and even less so with the π^* orbitals. Some insight may be gained from Figure 9a, which depicts the electronic structures of the **2b**(Fe^{III}) and **2b**(Fe^{IV}) isomers of HRP alongside those of P450 in the corresponding triplet states. The two states differ by a shift of a single electron from the corresponding a_{2u} orbital to the π^*_{xz} orbital. As can be seen, the a_{2u} orbital of the P450 species contain a large contribution of the sulfur σ-type hybrid pointing toward the iron,[6d,48d] while the same orbital for the HRP species is virtually a pure porphyrin orbital.[38,48] Consequently, shifting one electron away from a_{2u} in the P450 species converts the sulfur from a thiolate anion in **2b**(Fe^{IV}) partly to a thiolyl radical in **2b**(Fe^{III}). As shown in Figure 9b, this affects the Fe−S bonding, which is reduced from a two-electron bond in **2b**(Fe^{IV}) to a one-electron bond in **2b**(Fe^{III}).[45,48d] This reduction in the Fe−S bond order causes, in turn, significant Fe−S bond lengthening[6c] in the **2b**(Fe^{III}) isomer ($r_{Fe-S^-} = 2.53$ Å[6c]), compared with the **2b**(Fe^{IV}) isomer

(48) (a) Ogliaro, F.; de Visser, S. P.; Shaik, S. *J. Inorg. Biochem.* **2002**, *91*, 554−567. (b) Kumar, D.; de Visser, S. P.; Sharma, P. K.; Derat, E.; Shaik, S. *J. Biol. Inorg. Chem.* **2005**, *10*, 181−189. (c) de Visser, S. P.; Shaik, S.; Sharma, P. K.; Kumar, D.; Thiel, W. *J. Am. Chem. Soc.* **2003**, 125, 15779−15788. (d) Schöneboom, J. C.; Lin, H.; Reuter, N.; Thiel, W.; Cohen, S.; Ogliaro, F.; Shaik, S. *J. Am. Chem. Soc.* **2002**, *124*, 8142−8151.

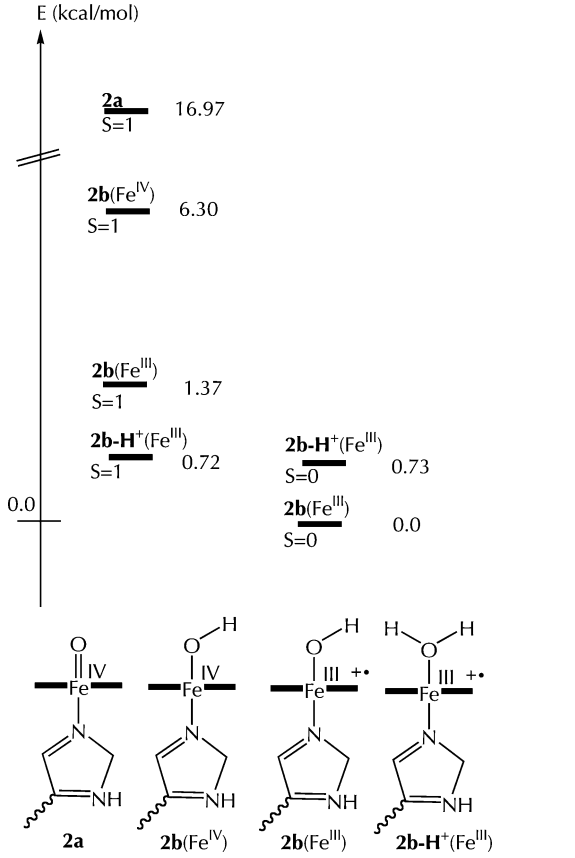

Figure 8. The various forms of Cpd II of HRP, arranged on an energy scale based on QM/MM data (B3//B1 data in kcal/mol).

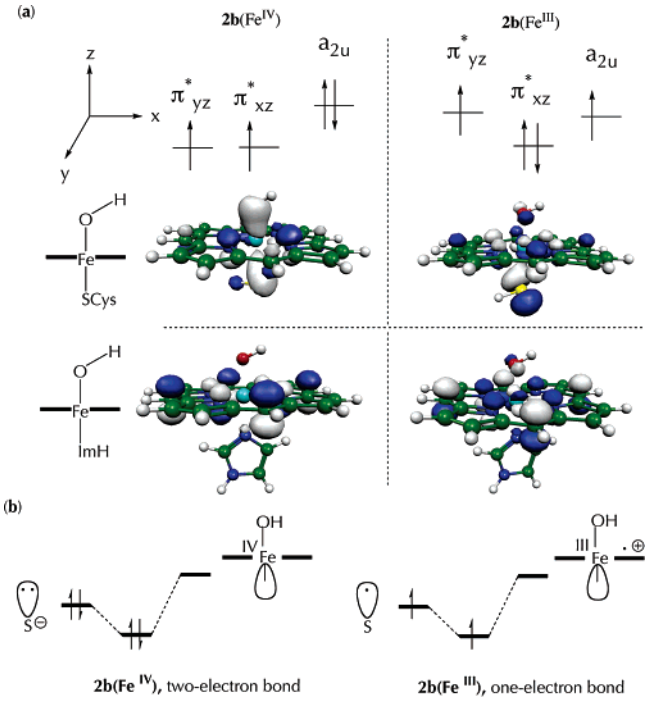

Figure 9. (a) Orbital occupancy for the **2b**(Fe^{IV}) and **2b**(Fe^{III}) isomers of HRP and P450. The corresponding a_{2u} natural orbitals for the two species are shown alongside the diagrams. (b) The Fe−S bond orbital in **2b**(Fe^{IV}) involves two-electron occupation, while in **2b**(Fe^{III}) it involves one-electron occupation (see ref 48d for a discussion).

(r_{Fe-S} = 2.33 Å[6c]), and destabilizes **2b**(Fe^{III}). By comparison, in HRP, the same electronic reorganization (shifting one electron

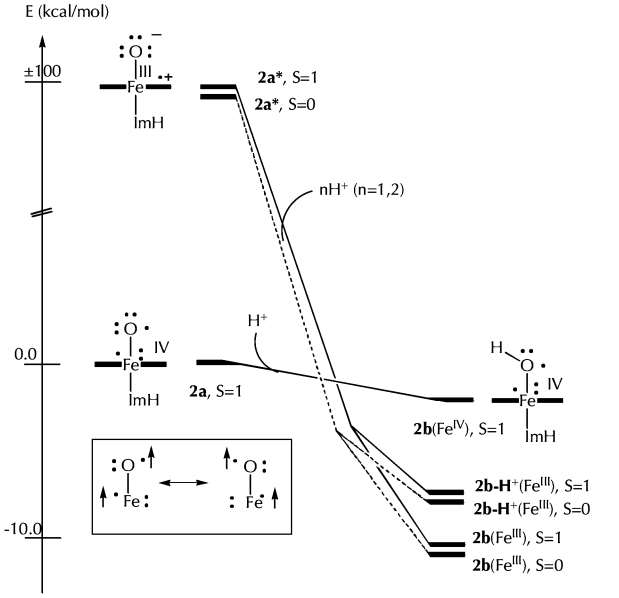

Figure 10. State-correlation diagram showing the origins of the isomers of Cpd II from the states of the primary species, **2a**.

from a_{2u} to π^*_{xz}) does not involve electron density change on the imidazole (Im) ligand, as may be seen from the almost identical Fe−N_{Im} bond lengths in the two HRP isomers (see Figures 1 and 3). As such, the **2b**(Fe^{III}) state of HRP does not suffer inherent destabilization compared with the **2b**(Fe^{IV}) isomer. The net result is that, in the case of P450, the **2b**(Fe^{III}) isomer is inherently somewhat less stable than **2b**(Fe^{IV}), while the opposite is true for HRP, where the **2b**(Fe^{III}) isomer is the more stable one. In both enzymes, the proteins stabilize preferentially the **2b**(Fe^{III}) isomers; the result is that in P450 these isomers become slightly more stable than **2b**(Fe^{IV}), while in HRP and other peroxidases the preferred stability of **2b**(Fe^{III}) over **2b**(Fe^{IV}) becomes significant.

Interrelationships and Origins of the Isomers of Cpd II of HRP. Figure 10 is a state correlation diagram that traces the origins of the various isomers of Cpd II to the states of the primary isomer, the oxo-ferryl species, **2a**. The unpaired electrons are shown schematically; the lone pairs are shown mostly on oxygen, and in the case of **2a** we show one d-lone pair on iron when necessary. To have the most compact representation, we chose to exhibit the structures using their principal covalent structure. Thus, for example, the state **2a** is represented with two unpaired electrons, one on oxygen and one on iron (in accord with the spin densities in, e.g., Figure 1). Of course, the full covalent state of **2a** has FeO bonding, analogous to the bonding in the triplet O_2 molecule,[49] and requires an equivalent form, as shown in the inset box near **2a**.

It is seen from Figure 10 that the only species that has a natural correlation (in terms of electronic structure) with **2a** is the hydroxo-ferryl **2b**(Fe^{IV}) isomer. This is indeed what the calculations show, namely that there is a contiguous energy path connecting the two species, as displayed above in Figure 5. All the other species, in which the iron is in the ferric oxidation state and the porphyrin is radical-cationic, i.e., **2b**(Fe^{III}) and **2b**-H^+(Fe^{III}), originate in a highly excited state of **2a**, designated

(49) For the bonding in O_2, see, for example: (a) Shaik, S.; Hiberty, P. C. *Rev. Comput. Chem.* **2004**, *20*, 1−100. (b) Moss, B. J.; Bobrowicz, F. W.; Goddard, W. A., III. *J. Chem. Phys.* **1975**, *63*, 4632−4639.

as **2a*** in Figure 10. To generate this excited state, one electron has to be shifted from the porphyrin ligand to one of the singly occupied π^* orbitals of **2a**. It is seen that, in **2a***, the oxygen atom gains one excess negative charge by comparison to the oxygen in **2a**. Indeed, the memory of this excess negative charge is retained in the isomers **2b**(Fe^{III}); for example, comparison of the oxygen charges in **2b**(Fe^{IV}) and **2b**(Fe^{III}) shows the latter to have a higher electronic charge, by approximately $0.4e^-$ (see Table S12 in the SI). Thus, the **2b**(Fe^{III}) and **2b-H**$^+$(Fe^{III}) isomers correlate to a high-energy state and are not naturally connected to the ground state of **2a**. We recall that our attempts to protonate **2a** and obtain **2b**(Fe^{III}) failed. This, in turn, means that **2b**(Fe^{III}) will be formed from **2a** at the expense of a significant barrier by crossover from one state surface to the other[50] or will be formed by internal electron transfer from the equilibrated **2b**(Fe^{IV}) electromer after the latter is formed.

The corresponding **2b-H**$^+$(Fe^{III}) isomers are also naturally connected to **2a***, in terms of their electronic structure, and can be formed either from protonation of the equilibrated **2b**(Fe^{III}) isomers or via double protonation from **2a** with a significant crossover barrier between the state surfaces. We recall that, in our computational scheme, we obtained the **2b-H**$^+$(Fe^{III}) isomers by attempting to convert **2b**(Fe^{III}) to **2a**. Thus, instead of losing one proton, to yield **2a**, the excess negative charge on the oxygen atom of **2b**(Fe^{III}) made this species basic enough (virtually an OH^- species) to abstract a proton from Arg_{38} and yield the ferric-aqua complexes.[50] Of course, the state of the deprotonated Arg_{38} is short-lived, and the normal state will be restored instantly (or even simultaneously) by protons from the surroundings. Finally, the correlation of the singlet-state species is highlighted by dashed lines to signify that these species must arise by spin-flip from the triplet states, and, hence, the interconnection between all the Cpd II isomers involves two-state reactivity, which is by now a common feature of the heme enzyme chemistry.[45,46]

On the basis of Figure 10 and the theoretical results, we can put together a chemical scenario that links all the isomers of HRP Cpd II, and this is shown in Scheme 4. It is seen that the primary species formed from Cpd I by reduction is **2a**. This species can then undergo facile protonation to yield the **2b**(Fe^{IV}) isomer. The ease of the protonation in the enzyme depends critically on the presence of the water molecule, labeled as W_{427} in Figures 3 and 4. *Without W_{427}, the distance between His_{42} and the oxo-iron moiety becomes too long, and the proton transfer will encounter a high barrier*. Another factor that determines the ease of protonation of **2a** is the pH: at a sufficiently basic pH, His_{42} will be deprotonated and the proton shuttle through W_{427} will be inefficient. Thus, **2a** can have sufficient lifetime to be probed only if W_{427} is absent and/or misplaced and under more basic conditions. Needless to say, the absence of W_{427} and/or the protonation state of His_{42} will change the hydrogen-bonding situation of **2a** and will, thereby, affect the Fe═O stretch frequency as observed in the resonance Raman studies.[14] Generally, the theoretically produced picture regarding **2a** and **2b**(Fe^{IV}) is in line with the conclusions of Andersson and Dawson.[16]

Once **2b**(Fe^{IV}) is formed, it is most likely that internal electron transfer from the porphyrin to the iron will be responsible for the **2b**(Fe^{III}) electromer in the triplet state. Thus, we may expect some equilibration of the two isomers. Once **2b**(Fe^{III}) is formed in a triplet state, this species can flip an electron spin and give rise to the singlet state of the **2b**(Fe^{III}) electromer,[51] hence two-state reactivity. An equilibration or coexistence of the **2b**(Fe^{IV}) and **2b**(Fe^{III}) isomers was reported in the synthetic heme models,[6a] and the fact that it has never been observed in HRP (or other enzymes) is puzzling.

Scheme 4. A Theoretically Based Reaction Scheme Showing Interconnections of the Isomers of Cpd II

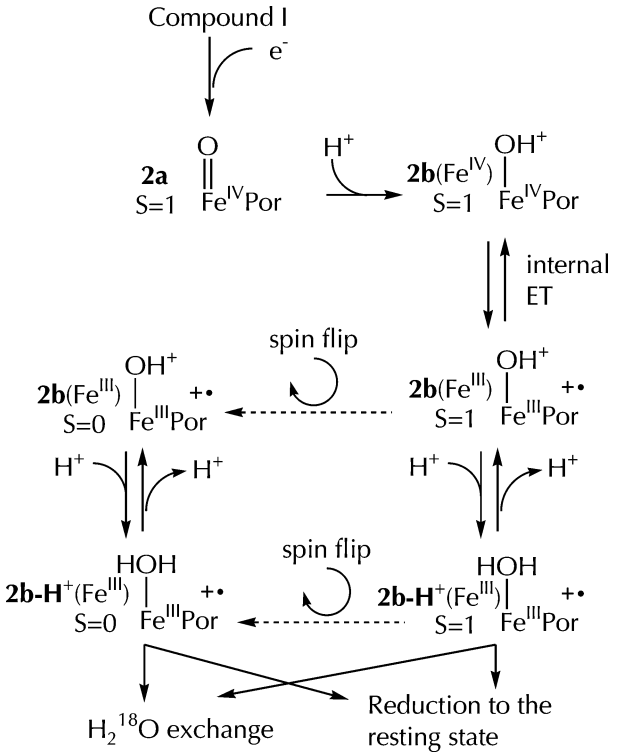

The final feature of note in Scheme 4 concerns the ferric-aqua isomers, **2b-H**$^+$(Fe^{III}). These species can be produced by further protonation of the **2b**(Fe^{III}) isomers ($S = 0, 1$). This second protonation will be slower than the first one (leading from **2b** to **2b**(Fe^{IV})), since the barrier that can be estimated from the energy scan for the formation of the **2b-H**$^+$(Fe^{III}) isomer (ca. 6 kcal/mol, see Figure S4 in the SI) is considerably larger than the barrier for the protonation that leads from **2b** to **2b**(Fe^{IV})), but still small enough to allow the protonation to happen (note that UB3LYP may be underestimating the protonation barriers). In addition, the generation of the aqua-ferric isomers will depend on the reprotonation of Arg_{38}, e.g., by proton supply from the surface of the protein (through His_{42} for example) or from the new H_2O_2 molecule that begins the cycle (Scheme 1). Our structural data for these isomers in Figure 7 show a long Fe−O bond, ca. 1.92 Å, *and suggest that this isomer might have been observed in the EXAFS experiments*

(50) While this state specificity may be an artifact of the mono-determinantal nature of the DFT wave function, and a higher level (currently unavailable) would have caused state mixing, still such a state mixing would have shown a significant barrier for the formation of **2b**(Fe^{III}) from **2a**.

(51) For spin flips in transition metal complexes, see: Danovich, D.; Shaik, S. *J. Am. Chem. Soc.* **1997**, *119*, 1773−1786. Thus, sufficient spin−orbit coupling interaction will be provided by mixing into the ground triplet state of **2b**(Fe^{III}) some character of the singlet excited state of **2b**(Fe^{III}), where the electron occupancy corresponds to $a_{2u}^1\,\pi^*_{xz}{}^1\,\pi^*_{yz}{}^2$ and the spins of the single electrons are paired to singlets. This mixing involves a shift of an electron between π^*_{xz} and π^*_{yz}, the mutually perpendicular d-orbitals; this, in turn, creates the angular momentum change necessary to flip a spin and convert **2b**(Fe^{III}), $S = 1$, to **2b**(Fe^{III}), $S = 0$.

of Chance et al.[9] Furthermore, the ferric-aqua isomers can easily exchange ^{18}O with bulk water, as observed by Kitagawa et al.,[15] using $H_2{}^{18}O$. Finally, the **2b**-**H**$^+$(Fe^{III}) electromers may undergo reductions easily and produce the ferric resting state[1] of the enzyme. Experimental evidence for such behavior is reflected in the reaction profile of Cpd II with substrates as a function of pH.[15a]

Concluding Remarks

QM and QM/MM calculations on Cpd II, the enigmatic active species in the catalytic cycle of HRP, reveal six low-lying states with different protonation states of the oxo ligand, different oxidation states of iron and porphyrin, and two different spin situations ($S = 0, 1$), as shown in Figure 10. The calculations provide us with sufficient insight to suggest a reactivity scheme for these isomeric forms and spin situations, detailed in Scheme 4. The primary form is **2a**, the oxo-ferryl form (PorFe^{IV}═O) that is generated from Cpd I by one-electron reduction. This isomer undergoes facile protonation and produces **2b**(Fe^{IV}), the hydroxo-ferryl isomer (PorFe^{IV}—OH$^+$) in the triplet state. The facility of this process depends critically on the presence of a water molecule, W_{427} in HRP (see Figures 3−6), and to some extent on the pH of the enzyme and the protonation state of His_{42}. In our opinion, and in accord with experimental reports in synthetic complexes,[6a] the **2b**(Fe^{IV}) electromer should be able undergo internal electron transfer from the porphyrin to the iron, to produce the triplet state of **2b**(Fe^{III}), the hydroxo-ferric electromer (Por$^{+\bullet}$Fe^{III}—OH). The latter can either flip a spin to produce the corresponding singlet-state species or/and undergo additional protonation to yield **2b**-**H**$^+$(Fe^{III}), the ferric-aqua porphyrin radical-cation complex. The latter complex can flip a spin to form the respective singlet state. Both forms of **2b**-**H**$^+$(Fe^{III}) can easily exchange a water molecule with the surroundings and/or undergo reduction to produce the resting state of HRP.

By contrast to this multi-form and rich reactivity scheme, revealed from theory, the known experimental data correspond only to **2a** and **2b**(Fe^{IV}). While for these isomers there is good agreement between theoretical and the experimentally derived features from structural[8−10] and spectroscopic[12−14,16,22] studies, the **2b**(Fe^{III}) states, and the "surprise" species **2b**-**H**$^+$(Fe^{III}), that are found in this study have never been observed for HRP or other heme enzymes. Moreover, all the spectroscopic studies, e.g., Mössbauer and resonance Raman, reveal only the presence of **2a**, while X-ray crystallography finds only **2b**(Fe^{IV}). Interestingly, however, whereas the most stable isomers, the **2b**(Fe^{III}) states, have never been reported for heme enzymes, such species were probed in the solution chemistry of synthetic heme models,[6a] and one may therefore hope that they can be characterized also for the enzyme. Similarly, while the "surprise" species, **2b**-**H**$^+$(Fe^{III}), have never been considered in heme chemistry, on the basis of the calculated Fe−O bond lengths we think that these isomers were, in fact, observed in the EXAFS studies of Chance et al.[9] Furthermore, on the basis of the calculated features, we consider that the exchange of ^{18}O (from $H_2{}^{18}O$) that was reported for Cpd II HRP[15c] originates from these "surprise" species that are ferric-aqua complexes with long and weak Fe−O bonds that may allow facile exchange of the water ligand. It is clear, therefore, that the role of Cpd II in the HRP cycle is considerably more multi-faceted than has been revealed so far by the variety of experimental techniques. It is very likely that the six species exist in different pH ranges in the enzyme, and their function in substrate oxidation may be different. We hope that our suggested Scheme 4 and calculated Mössbauer parameters for all the isomers may be helpful toward eventual characterization of these missing isomers of Cpd II.

Finally, a sober note of caution is necessary in view of the occasional limited accuracy of the DFT methods. Clearly, high-level ab initio calculations will be required eventually to assess the relative energies of various isomers of Cpd II in the catalytic cycle of HRP and other peroxidases. Despite this caveat, the qualitative conclusions based on Figures 9 and 10 should remain valid because they reflect the essential electronic reorganization during the transformation of the isomers.

Acknowledgment. This research was supported by the German Federal Ministry of Education and Research (BMBF) within the framework of the German-Israeli Project Cooperation (DIP). The authors thank F. Neese for making his program ORCA available.

Supporting Information Available: Energies and coordinates for all species, as well as spin densities and charges, and refs 30, 32, and 35 in full. This material is available free of charge via the Internet at http://pubs.acs.org.

JA0600734